Model. Sim. Mater. Sci. Eng. resubmitted (2012)

Computing dislocation stress fields in anisotropic elastic media using fast multipole expansions

Jie Yin[1], D. M. Barnett[1,2], S. P. Fitzgerald[3] and Wei Cai[2]

[1]Department of Materials Science and Engineering, Stanford University, Stanford, CA 94305, USA

[2]Department of Mechanical Engineering, Stanford University, Stanford, CA 94305, USA

[3]EURATOM/CCFE Fusion Association, Culham Science Centre, Abingdon, OX14 3DB, UK

Abstract. The calculation of stress fields due to dislocations and hence the forces they exert on each other is the most time consuming step in dislocation dynamics (DD) simulations. The fast multipole method (FMM) can reduce the computational cost at each simulation step from $\mathcal{O}(N^2)$ to $\mathcal{O}(N)$ for an ensemble of N dislocation segments. However, FMM has not yet been applied to three dimensional DD simulations which take into account anisotropic elasticity. We demonstrate a systematic procedure to establish this capability by first obtaining the derivatives of the elastic Green's function to arbitrary order for a medium of general anisotropy. We then compute the stress field of a dislocation loop using multipole expansions based on these derivatives, and analyze the dependence of numerical errors on the expansion order. This method can be implemented in large scale DD simulations when the consideration of elastic anisotropy is necessary, for example the technologically important cases of iron and ferritic steels at high temperatures.

1. Introduction

The behavior of dislocations governs the mechanical properties of crystalline materials. By studying the evolution of dislocation microstructure, dislocation dynamics (DD) simulations aim to link the plastic deformation of single crystals with the microscopic dynamics of individual dislocations. In DD simulations, the dislocation lines are discretized, and can be represented as a set of nodes connected by short straight segments. Distant dislocation segments interact via long-range Peach-Koehler forces, and the calculation of these interactions can pose a severe computational challenge for large systems. For a system in which the total number of dislocation segments is N, the computational complexity scales as N^2 and is hence very CPU-intensive. The fast multipole method (FMM) can reduce the computational cost to $\mathcal{O}(N)$ [1]. Using isotropic elasticity, LeSar and Rickman performed a multipole expansion of the interaction energy between dislocations in three dimensions [2], and Wang *et al.* gave multipole representations of the elastic fields of dislocation loop ensembles [3]. Based on LeSar's and Wang's mathematical framework, Arsenlis *et al.*

implemented the FMM algorithm into their Parallel Dislocation Simulator (ParaDiS) code, enabling large scale DD simulations to study the plastic behavior of single crystals [4]. Recently Zhao *et al.* implemented the new version of FMM [5] yielding accelerated stress field calculations [6].

However, all the implementations mentioned above are based on isotropic elasticity, while real single crystals are in many cases anisotropic. Under certain conditions, *e.g.* α-iron at high temperature [7], isotropic elasticity fails completely, and can no longer be used to describe the system. There is generally no explicit closed-form expression for the stress field of a dislocation segment in anisotropic elasticity, and the evaluation of remote dislocation interactions typically involves the numerical calculation of an integral, or the solution of an eigenvalue problem [8]. Therefore, anisotropic elasticity-based DD simulations are much slower than the relatively efficient isotropic DD codes (e.g. by a factor of about 200 [9]), so the implementation of the FMM is particularly advantageous in this case.

Pang derived the interaction energy between two infinitely long parallel straight dislocations using anisotropic elasticity, and implemented the FMM for two-dimensional DD simulations [11]. However, for dislocation configurations of arbitrary geometric complexity three dimensions are required, and to this end we describe here an FMM implementation suitable for this task.

The FMM for DD simulations requires the derivatives of the anisotropic elastic Green's function. For this purpose, we develop a systematic procedure to calculate these derivatives to arbitrary order, which is detailed in Appendix A. The numerical algorithms to compute the Green's function derivatives are described in Appendix B and Appendix C. Based on these results, we perform a multipole expansion of the dislocation stress field, which is described in Section 2. In Section 3 we evaluate the accuracy of our FMM implementation scheme by studying the effect of expansion orders and investigating discontinuities at field cell boundaries.

2. Method

2.1. Taylor and multipole expansions

In an infinite homogeneous linear elastic medium with elastic stiffness tensor C_{ijkl}, the stress $\boldsymbol{\sigma}$ at $\boldsymbol{x}$ due to a dislocation loop L is given by Mura's formula [12, 13]:

$$\sigma_{ij}(\boldsymbol{x}) = C_{ijkl} \oint_L \epsilon_{lnh} C_{pqmn} G_{kp,q}(\boldsymbol{x} - \boldsymbol{x'}) b_m \mathrm{d}x'_h \tag{1}$$

where ϵ_{lnh} is the permutation tensor, and $G_{kp,q}$ is the first derivative of the Green's function G_{kp} with respect to x_q. Only closed loops define $\boldsymbol{\sigma}$ uniquely, but one can perform the above integral along a straight finite segment and then sum contributions to determine the unique field due to a discretized closed polygonal loop.

In isotropic media, equation (1) can be reduced to the following line integral:

$$\sigma_{ij}(\boldsymbol{x}) = \frac{\mu b_n}{8\pi} \int R_{,mpp}(\boldsymbol{x} - \boldsymbol{x'}) \left[\epsilon_{jmn} \mathrm{d}x'_i + \epsilon_{imn} \mathrm{d}x'_j \right]$$

$$+\frac{\mu b_n}{4(1-\nu)\pi}\int \epsilon_{kmn}\left[R_{,ijm}(\boldsymbol{x}-\boldsymbol{x'})-\delta_{ij}R_{,ppm}(\boldsymbol{x}-\boldsymbol{x'})\right]\mathrm{d}x'_k \qquad (2)$$

where $R_{,ijk}=\frac{\partial}{\partial x_i}\frac{\partial}{\partial x_j}\frac{\partial}{\partial x_k}R$, $R=|\boldsymbol{x}-\boldsymbol{x'}|$. The FMM scheme of Arsenlis *et al.* [4] is based on Taylor expansions of equation (2).

Similarly, we perform Taylor expansions of equation (1) as follows. Consider a differential segment $\mathrm{d}\boldsymbol{x'}$ with Burgers vector $\boldsymbol{b}$, whose stress field at a point $\boldsymbol{x}$ is $\mathrm{d}\sigma_{ij}(\boldsymbol{x})$,

$$\mathrm{d}\sigma_{ij}(\boldsymbol{x}) = C_{ijkl}\mathrm{d}\epsilon_{kl}(\boldsymbol{x}) \qquad (3)$$

$$\mathrm{d}\epsilon_{kl}(\boldsymbol{x}) = \epsilon_{lnh}C_{pqmn}b_m\mathrm{d}x_h G_{kp,q}(\boldsymbol{x}-\boldsymbol{x'}) \qquad (4)$$

where $\mathrm{d}\epsilon_{kl}(\boldsymbol{x})$ is the differential strain field at $\boldsymbol{x}$. Suppose $\mathrm{d}\boldsymbol{x'}$ and $\boldsymbol{x}$ lie in different cells, whose centers are $\boldsymbol{x''}$ and $\boldsymbol{x'''}$ respectively, as shown in Fig. 1.

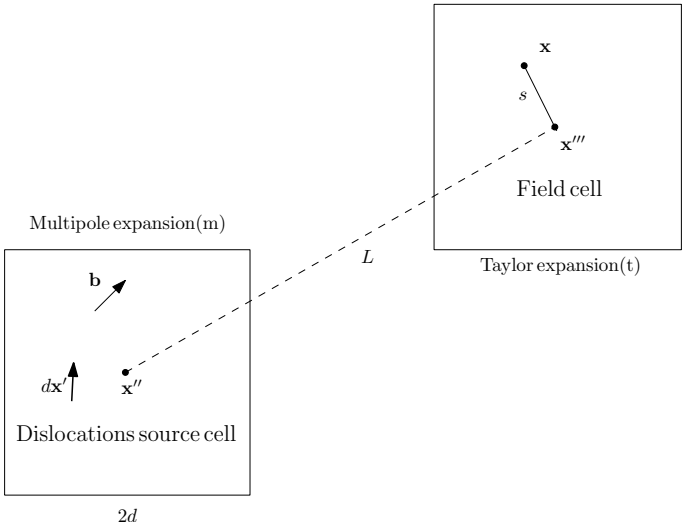

Figure 1. Differential segment $\mathrm{d}\boldsymbol{x'}$ is located in the source cell centered at $\boldsymbol{x''}$ and the Burgers vector is $\boldsymbol{b}$. The field point $\boldsymbol{x}$ is in the field cell centered at $\boldsymbol{x'''}$. Both cells have length $2d$. The distance between two cell centers is L. We perform multipole expansions for the source cell and Taylor expansion for the field cell.

By performing a Taylor expansion of $G_{kp,q}(\boldsymbol{x}-\boldsymbol{x'})$ for $\boldsymbol{x}$ near $\boldsymbol{x'''}$, we arrive at

$$\mathrm{d}\epsilon_{kl}(\boldsymbol{x}) = \sum_{\zeta=0}^{\infty}\frac{1}{\zeta!}\sum_{\alpha+\beta+\gamma=\zeta}\frac{\zeta!}{\alpha!\,\beta!\,\gamma!}\epsilon_{lnh}C_{pqmn}b_m\mathrm{d}x'_h\cdot(x_1-x'''_1)^{\alpha}(x_2-x'''_2)^{\beta}(x_3-x'''_3)^{\gamma}$$
$$\left[\left(\frac{\partial}{\partial x_1}\right)^{\alpha}\left(\frac{\partial}{\partial x_2}\right)^{\beta}\left(\frac{\partial}{\partial x_3}\right)^{\gamma}G_{kp,q}(\boldsymbol{x}-\boldsymbol{x'})\right]_{\boldsymbol{x}=\boldsymbol{x'''}} \qquad (5)$$

Defining

$$M^{\alpha\beta\gamma} \equiv \frac{(\alpha+\beta+\gamma)!}{\alpha!\,\beta!\,\gamma!} \qquad (6)$$

$$\mathrm{d}\epsilon^{\alpha\beta\gamma}_{kl}(\boldsymbol{x'''}) \equiv \epsilon_{lnh}\,C_{pqmn}b_m\mathrm{d}x'_h\,G^{\alpha,\beta,\gamma}_{kp,q}(\boldsymbol{x'''}-\boldsymbol{x'}) \qquad (7)$$

$$G^{\alpha,\beta,\gamma}_{kp,q}(\boldsymbol{x'''}-\boldsymbol{x'}) \equiv \left[\left(\frac{\partial}{\partial x_1}\right)^{\alpha}\left(\frac{\partial}{\partial x_2}\right)^{\beta}\left(\frac{\partial}{\partial x_3}\right)^{\gamma}G_{kp,q}(\boldsymbol{x}-\boldsymbol{x'})\right]_{\boldsymbol{x}=\boldsymbol{x'''}}, \qquad (8)$$

equation (5) becomes

$$\mathrm{d}\epsilon_{kl}(\boldsymbol{x}) = \sum_{\zeta=0}^{\infty} \frac{1}{\zeta!} \sum_{\alpha+\beta+\gamma=\zeta} M^{\alpha\beta\gamma} \cdot \mathrm{d}\epsilon_{kl}^{\alpha\beta\gamma}(\boldsymbol{x'''}) \cdot (x_1 - x_1''')^{\alpha}(x_2 - x_2''')^{\beta}(x_3 - x_3''')^{\gamma} \quad (9)$$

Using a Taylor expansion for $\boldsymbol{x'}$ near $\boldsymbol{x''}$, equation (7) becomes

$$\mathrm{d}\epsilon_{kl}^{\alpha\beta\gamma}(\boldsymbol{x'''}) = \epsilon_{lnh} C_{pqmn} b_m \mathrm{d}x_h' \sum_{\xi=0}^{\infty} \frac{1}{\xi!} \sum_{a+b+c=\xi} M^{abc} \cdot (x_1' - x_1'')^a (x_2' - x_2'')^b (x_3' - x_3'')^c \left[\left(\frac{\partial}{\partial x_1'}\right)^a \left(\frac{\partial}{\partial x_2'}\right)^b \left(\frac{\partial}{\partial x_3'}\right)^c G_{kp,\,q}^{\alpha,\,\beta,\,\gamma}(\boldsymbol{x'''} - \boldsymbol{x'}) \right]_{\boldsymbol{x'}=\boldsymbol{x''}} \quad (10)$$

Note that $\partial/\partial x = -\partial/\partial x'$ and define the differential multipole moment

$$\mathrm{d}\eta_{mh}^{abc}(\boldsymbol{x''}) = b_m \mathrm{d}x_h' \cdot (x_1' - x_1'')^a (x_2' - x_2'')^b (x_3' - x_3'')^c. \quad (11)$$

Then equation (10) can be rewritten as

$$\begin{aligned} \mathrm{d}\epsilon_{kl}^{\alpha\beta\gamma}(\boldsymbol{x'''}) &= \epsilon_{lnh} C_{pqmn} \sum_{\xi=0}^{\infty} \frac{(-1)^{\xi}}{\xi!} \sum_{a+b+c=\xi} M^{abc} \cdot \mathrm{d}\eta_{mh}^{abc}(\boldsymbol{x''}) \\ &\quad \left[\left(\frac{\partial}{\partial x_1}\right)^a \left(\frac{\partial}{\partial x_2}\right)^b \left(\frac{\partial}{\partial x_3}\right)^c G_{kp,\,q}^{\alpha,\,\beta,\,\gamma}(\boldsymbol{x} - \boldsymbol{x''}) \right]_{\boldsymbol{x}=\boldsymbol{x'''}} \\ &= \epsilon_{lnh} C_{pqmn} \sum_{\xi=0}^{\infty} \frac{(-1)^{\xi}}{\xi!} \sum_{a+b+c=\xi} M^{abc} \cdot \mathrm{d}\eta_{mh}^{abc}(\boldsymbol{x''}) \\ &\quad G_{kp,q}^{a+\alpha,\,b+\beta,\,c+\gamma}(\boldsymbol{x'''} - \boldsymbol{x''}). \end{aligned} \quad (12)$$

Because $\mathrm{d}\eta_{mh}^{abc}$ is called the multipole moment, we will refer to the above expansion around the source cell center $\boldsymbol{x''}$ as the multipole expansion. Equation (12) thus describes the mapping from multipole expansion coefficients ($\mathrm{d}\eta_{mh}^{abc}$) to Taylor expansion coefficients ($\mathrm{d}\epsilon_{kl}^{\alpha\beta\gamma}$). Now integrate the strain field contribution $\mathrm{d}\epsilon_{kl}$ from differential segments $\mathrm{d}\boldsymbol{x'}$ along the dislocation line, and multiply by the elastic stiffness tensor to obtain

$$\begin{aligned} \sigma_{ij}(\boldsymbol{x}) &= C_{ijkl} \int \mathrm{d}\epsilon_{kl}(\boldsymbol{x}) \\ &= C_{ijkl} \sum_{\zeta=0}^{\infty} \frac{1}{\zeta!} \sum_{\alpha+\beta+\gamma=\zeta} M^{\alpha\beta\gamma} \epsilon_{kl}^{\alpha\beta\gamma}(\boldsymbol{x'''}) \, (x_1 - x_1''')^{\alpha}(x_2 - x_2''')^{\beta}(x_3 - x_3''')^{\gamma} \end{aligned} \quad (13)$$

where

$$\begin{aligned} \epsilon_{kl}^{\alpha\beta\gamma}(\boldsymbol{x'''}) &= \int \mathrm{d}\epsilon_{kl}^{\alpha\beta\gamma}(\boldsymbol{x'''}) \\ &= \epsilon_{lnh} C_{pqmn} \sum_{\xi=0}^{\infty} \frac{(-1)^{\xi}}{\xi!} \sum_{a+b+c=\xi} M^{abc} \eta_{mh}^{abc}(\boldsymbol{x''}) \, G_{kp,\,q}^{a+\alpha,\,b+\beta,\,c+\gamma}(\boldsymbol{x'''} - \boldsymbol{x''}) \end{aligned} \quad (14)$$

$$\begin{aligned} \eta_{mh}^{abc}(\boldsymbol{x''}) &= \int \mathrm{d}\eta_{mh}^{abc}(\boldsymbol{x''}) \\ &= \int (x_1' - x_1'')^a (x_2' - x_2'')^b (x_3' - x_3'')^c \, b_m \mathrm{d}x_h' \end{aligned} \quad (15)$$

2.2. Algorithm

In summary, the stress field at $\boldsymbol{x}$ in a cell centered at $\boldsymbol{x'''}$ due to dislocation segments in a cell centered at $\boldsymbol{x''}$ can be computed using the following 4 steps. To avoid loss of accuracy in numerical implementation, we introduce scaled variables (e.g. $\tilde{\eta}^{abc}_{mh}$) scaling by the half cell size d.

Step 1. Compute multipole moments at source cell center $\boldsymbol{x''}$:

$$\tilde{\eta}^{abc}_{mh}(\boldsymbol{x''}) \equiv \frac{\eta^{abc}_{mh}(\boldsymbol{x''})}{d^{a+b+c}} = \int \left(\frac{x'_1 - x''_1}{d}\right)^a \left(\frac{x'_2 - x''_2}{d}\right)^b \left(\frac{x'_3 - x''_3}{d}\right)^c b_m \mathrm{d}x'_h \tag{16}$$

Step 2. Compute Taylor expansions of the strain field at field cell center $\boldsymbol{x'''}$:

$$\begin{aligned}\tilde{\epsilon}^{\alpha\beta\gamma}_{kl}(\boldsymbol{x'''}) &\equiv \epsilon^{\alpha\beta\gamma}_{kl}(\boldsymbol{x'''}) \cdot d^{\alpha+\beta+\gamma} \\ &= \sum_{\xi=0}^{\infty} \frac{(-1)^\xi}{\xi!} \sum_{a+b+c=\xi} M^{abc}\, \tilde{\eta}^{abc}_{mh}(\boldsymbol{x''}) \cdot \tilde{g}_{klmh}(a,b,c,\alpha,\beta,\gamma,\boldsymbol{x''},\boldsymbol{x'''})\end{aligned} \tag{17}$$

where

$$\tilde{g}_{klmh}(a,b,c,\alpha,\beta,\gamma,\boldsymbol{x''},\boldsymbol{x'''}) = \epsilon_{lnh} C_{pqmn} \cdot d^{\xi+\zeta} \cdot G^{a+\alpha,\,b+\beta,\,c+\gamma}_{kp,q}(\boldsymbol{x'''} - \boldsymbol{x''}) \tag{18}$$

is the kernel that converts multipole expansion coefficients $\tilde{\eta}_{mh}$ in the source cell to Taylor expansion coefficients $\tilde{\epsilon}_{kl}$ in the field cell, and

$$\xi = a + b + c$$
$$\zeta = \alpha + \beta + \gamma$$

Step 3. Compute the strain field at $\boldsymbol{x}$:

$$\epsilon_{kl}(\boldsymbol{x}) = \sum_{\zeta=0}^{\infty} \frac{1}{\zeta!} \sum_{\alpha+\beta+\gamma=\zeta} M^{\alpha\beta\gamma}\, \tilde{\epsilon}^{\alpha\beta\gamma}_{kl}(\boldsymbol{x'''}) \left(\frac{x_1 - x'''_1}{d}\right)^\alpha \left(\frac{x_2 - x'''_2}{d}\right)^\beta \left(\frac{x_3 - x'''_3}{d}\right)^\gamma \tag{19}$$

Step 4. Compute the stress field at $\boldsymbol{x}$:

$$\sigma_{ij}(\boldsymbol{x}) = C_{ijkl}\, \epsilon_{kl}(\boldsymbol{x}) \tag{20}$$

Steps 1 to 4 can be implemented numerically. The kernel $\tilde{g}_{klmh}$ is proportional to spatial derivatives of the Green's function

$$\begin{aligned}&G^{a+\alpha,\,b+\beta,\,c+\gamma}_{kp,q}(\boldsymbol{x'''} - \boldsymbol{x''}) \\ &= \left[\left(\frac{\partial}{\partial x_1}\right)^{a+\alpha} \left(\frac{\partial}{\partial x_2}\right)^{b+\beta} \left(\frac{\partial}{\partial x_3}\right)^{c+\gamma} \frac{\partial}{\partial x_q}\, G_{kp}(\boldsymbol{x} - \boldsymbol{x''})\right]_{\boldsymbol{x}=\boldsymbol{x'''}}\end{aligned} \tag{21}$$

Derivations and numerical implementations of the derivatives of the Green's function are presented in the Appendices. According to equation (A.16), $G^{a+\alpha,\,b+\beta,\,c+\gamma}_{kp,q}(\boldsymbol{x'''} - \boldsymbol{x''})$ scales as $1/L^{\xi+\zeta+2}$, where $L = |\boldsymbol{x'''} - \boldsymbol{x''}|$. Therefore, $d^{\xi+\zeta} \cdot G^{a+\alpha,\,b+\beta,\,c+\gamma}_{kp,q}(\boldsymbol{x'''} - \boldsymbol{x''})$ is well behaved for arbitrarily high expansion order as long as $L > 2d$, i.e. when the field cell and the source cell do not overlap.

2.3. Truncation of expansion order

The previous section did not define the numerical implementation completely, because the summations in equations (17) and (19) still include an infinite number of terms. In practice, we must limit the order of the multipole expansion $\xi \equiv a+b+c$ by a maximum value m, and the order of the Taylor expansion $\zeta \equiv \alpha+\beta+\gamma$ by a maximum value t. Several truncation schemes exist in the literature.

A simple way to introduce this truncation is to replace the summation in equation. (17) by $\sum_{\xi=0}^{m}$, and to replace the summation in equation (19) by $\sum_{\zeta=0}^{t}$. This means that for each multipole moment of order up to m at the center of the source cell, the Taylor expansion of its strain field of order up to t will be computed at the center of the field cell. This requires the availability of the derivatives of the Green's functions of order up to $m+t+1$, as illustrated in Fig. 2(a). Suppose that the derivatives of the Green's function are available up to order $p+1$, one still has the freedom to choose the individual values for m and t within the constraint of $m+t=p$. Intuitively, we expect the optimal choice that gives the lowest error would correspond to the case of $m \approx t$. Although this truncation scheme has been used before in DD simulations [4], strictly speaking it is not a correct multipole expansion at a given order (p), as explained below.

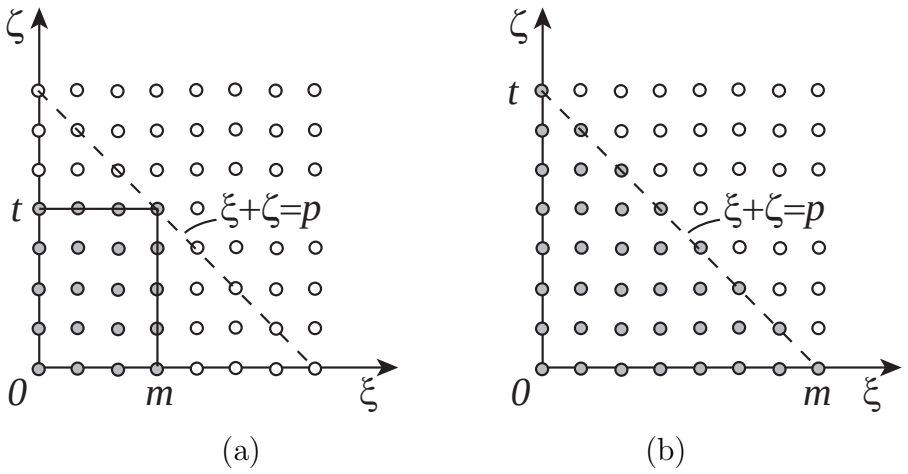

Figure 2. (a) In the first truncation scheme, the multiple expansion order satisfies $\xi \in [0, m]$ and the Taylor expansion order satisfies $\zeta \in [0, t]$. This requires Green's function derivatives up to $(p+1)$-th order, where $p = m+t$. (b) In the second truncation scheme, all combinations of ξ and ζ that satisfy $0 \le \xi+\zeta \le p$ are included, so that $m = t = p$. Filled circles represent terms included in the expansion, and open circles represent terms that are not included.

The correct way [2] to truncate the expansions at a given order p is to include all combinations of ξ and ζ that satisfy $0 \le \xi+\zeta \le p$, as shown in Fig. 2(b). In this case, both the maximum multipole expansion order m and the maximum Taylor expansion order t equal p. Operationally, this means that the summation in equation (19) is replaced by $\sum_{\zeta=0}^{p}$, while the summation in equation (17) is replaced by $\sum_{\xi=0}^{p-\zeta}$. In other words, the maximum

order to which we Taylor expand the strain field due to a dislocation multipole depends on the order of this multipole.

We have implemented both truncation schemes and found that, given the same derivatives of the Green's function up to order $p+1$, the second truncation scheme always gives lower error (by more than a factor of 4 in our test cases) than the first truncation scheme (even for the optimal choice of m and t). This can be understood by noticing that all terms in the expansion with different ξ and ζ but the same $\xi+\zeta=p$ are of the same order.‡ All terms of the same order must be included in order to reach accuracy of that order. Hence the scheme in Fig. 2(a) is only accurate to order $\min(m,t)$, while the the scheme in Fig. 2(b) is accurate to order p, even though they both make use of Green's function derivatives up to order $p+1$. Therefore, the scheme shown in Fig. 2(b) is not only preferred, but is the correct way to truncate the multipole expansions. It is used for the rest of this paper.

Note that the Green's function derivatives only need be evaluated at $\boldsymbol{x'''}-\boldsymbol{x''}$, i.e. the distance vector between cell centers. In the FMM scheme of [4], there are less than $6^3=216$ distinct directions for the $\boldsymbol{x'''}-\boldsymbol{x''}$ vectors (this number can be further reduced by taking symmetry into account). The Green's function derivatives along these directions can be pre-computed before running DD simulations.

3. Results

We implemented the algorithm described above using Matlab [14]. To evaluate the results given by the fast multipole expansions, we computed the stress field due to a dislocation loop and compared it with direct calculations obtained using our DDLab code based on anisotropic elasticity [9] (using the Willis-Steeds-Lothe formula [10]).

Given pre-computed derivatives of the Green's function up to order $n=p+1$, both the multipole expansion order $\xi=a+b+c$ and the Taylor expansion order $\zeta=\alpha+\beta+\gamma$ range from 0 to p. However, for a given multipole moment of order ξ, the Taylor expansion of its strain field is only evaluated up to order $p-\xi$. The source and field cells are both cubes of side $2d$, where d is chosen to be $500\,\mathring{A}$. The distance between the two cell centers is $L=|\boldsymbol{x'''}-\boldsymbol{x''}|$.

The multipole expansion results are expected to converge to the exact solution in the limit of $L/d\gg 1$, i.e. when the two cells are well separated. For the same reason, the largest error is expected for cells with the smallest value of L/d. In its three dimensional isotropic FMM implementation, ParaDiS [4] adopts a hierarchical grid structure. As shown in Fig.3(a), the smallest distance between a field cell and a source cell is $L=4d$, for which $(\boldsymbol{x'''}-\boldsymbol{x''})$ is along the $[1\,0\,0]$ direction. We choose this geometry as one of our test cases. To be specific, we choose $\boldsymbol{x''}=[0,0,0]$ and $\boldsymbol{x'''}=[L,0,0]$, with $L=4d$. For comparison

‡ The second truncation scheme will also look more natural if we derive the multipole expansions in a different way. Starting from equation (1), instead of performing a Taylor expansion twice, for $\boldsymbol{x'}$ and $\boldsymbol{x}$, respectively, we can perform one Taylor expansion for $\boldsymbol{x}-\boldsymbol{x'}$ around $\boldsymbol{x'''}-\boldsymbol{x''}$. Truncating this Taylor expansion at order p corresponds to Fig. 2(b).

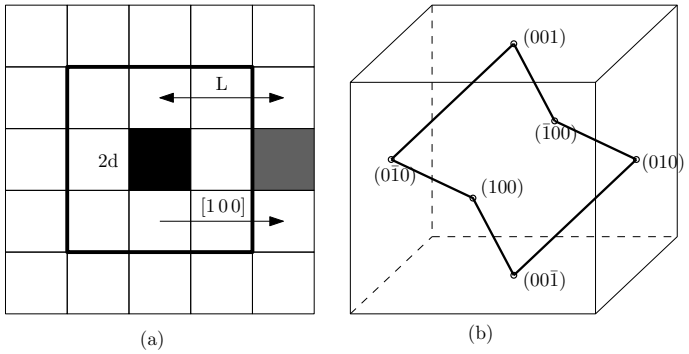

Figure 3. (a) Cell geometries for FMM implementation in ParaDiS [4]. All cells have length $2d$ and the source cell is in black. Cells that are nearest neighbors of the source cell (i.e. within the square in thick lines) are not included in the multipole expansion at the current level. The closest field cell (gray) included in the multipole expansion corresponds to $L = 4d$. (b) A hexagonal dislocation loop connecting all six face centers of the source cell.

purposes, we also consider another test case in which $L = 40d$. In both cases, the Green's function derivatives only need to be computed along the direction of $[1\,0\,0]$. For a given direction, the n-th order derivative of the Green's function is proportional to $1/r^{n+1}$, where r is the distance between source point and field point, see equation (A.16).

We consider two anisotropic crystals, molybdenum (Mo, c_{44}=110 GPa, c_{11}=460 GPa, c_{12}=176GPa, anisotropy ratio $A = 0.72$) and sodium (Na, $c_{11} = 6.03$ GPa, $c_{12} = 4.59$ GPa, $c_{44} = 5.86$ GPa, anisotropy ratio $A = 8.15$).§ We pre-computed the derivatives of the Green's function up to the 8-th order for Mo and 12-th order for Na. The derivatives are computed based on the integral formalism (see Appendix A) with 21 integration points for Mo and 41 integration points for Na.

The source cell contains a hexagonal dislocation loop connecting all six face centers, as shown in Fig.3(c). The dislocation Burgers vector is $\boldsymbol{b} = [-0.5, 2, 3]\mathring{A}$‖ We examine the stress field along a line within the field cell defined by $\boldsymbol{x'} = \boldsymbol{x'''} + \boldsymbol{s_0} \cdot s$, where $\boldsymbol{s_0} = [1, 0, 0]$ and $-d < s < d$. To evaluate the accuracy of the multipole expansion method, we need to consider the following factors: maximum multipole/Taylor expansion order p, and the separation ratio L/d. These are discussed below.

3.1. Relative error in stress

Fig.4(a) plots σ_{xy} as a function of s for different values of maximum expansion order n, for the case of Mo with $L/d = 4$. The exact solution based on the Willis-Steeds-Lothe (WSL)

§ Mo can be considered as moderately anisotropic while Na is highly anisotropic. We note that as the temperature approaches the $\alpha - \gamma$ phase transition temperature of iron, the anisotropy ratio of Fe can approach 7.4, comparable to the anisotropy ratio of Na.

‖ The choice of such an unphysical Burgers vector is to ensure that our test case is fairly general, e.g. every dislocation segment has both edge and screw components.

formula [9] is also shown for comparison. Notice that for $p = 1$, the computed stress field is a constant (instead of being a linear function of space) within the field cell. This is due to the monopole ($\zeta = 0$) coefficient being zero in the source cell, which contains a complete dislocation loop. With increasing p, the multipole expansion results quickly converge to the exact solution. To quantify the effect of expansion order, we define the maximum relative error of all stress components

$$\mathrm{RE} = \frac{||\sigma_{ij} - \sigma_{ij}^{\mathrm{WSL}}||}{||\sigma_{ij}^{\mathrm{WSL}}||} \tag{22}$$

The relative errors for both $L = 4d$ and $L = 40d$ cases are summarized in Fig.4(b). The maximum relative error RE decreases exponentially) with increasing p. The error for the case of $L = 40d$ is also much smaller than that for $L = 4d$, as it should be.

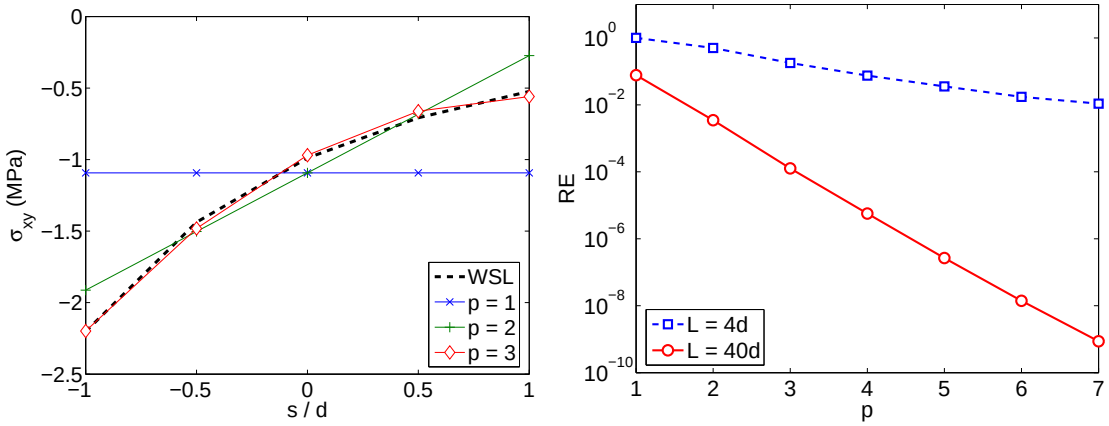

Figure 4. (a) σ_{xy} as a function of s for $d = L/4$, and different maximum expansion order p. (b) RE as a function of p for $L = 4d$ and $L = 40d$.

3.2. Discontinuity at field cell boundaries

The relative errors considered above are limited to field points within a single field cell. As the field point goes from one field cell to its neighbor, the stress field is evaluated as a Taylor expansion around a different cell center. This causes a discontinuity in the FMM stress field across cell boundaries.¶ As a result, a dislocation moving across FMM cell boundaries may experience a jump in the Peach-Koehler force, which is a numerical artifact that needs to be minimized. Here we investigate the stress continuity at cell boundaries for different values of maximum expansion order n.

¶ In principle, this discontinuity can be removed by an interpolation scheme that evaluates the stress field based on Taylor expansion coefficients in neighboring cells. Because we found that the discontinuity is about the same as the relative error and decreases rapidly with expansion order n, this possibility is not explored in this work.

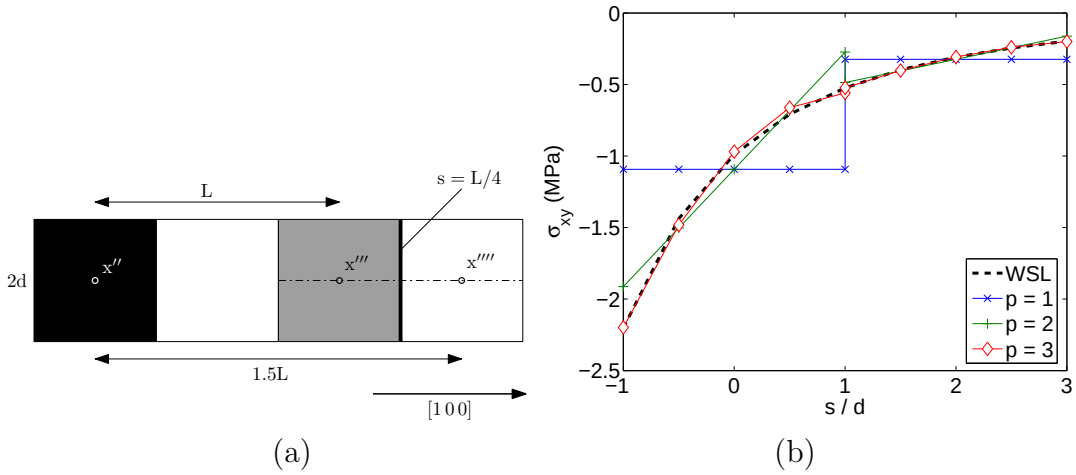

Figure 5. (a) Setup for the boundary continuity study where $L = 4d$. The field point moves along the dash-dotted line, *i.e.* s goes from $-d$ to $3d$. (b) σ_{xy} as a function of s for different maximum expansion order p.

In this test case, $L = 4d$, and the field point moves along $[1\,0\,0]$ direction and s goes from $-d$ to $3d$, as shown in Fig.5(a). When $-d \leq s \leq d$, the stress field at $\boldsymbol{x}$ is obtained from a Taylor expansion around cell center $\boldsymbol{x'''} = [4d, 0, 0]$. When $d \leq s \leq 3d$, the stress field at $\boldsymbol{x}$ is obtained from a Taylor expansion around cell center $\boldsymbol{x''''} = [6d, 0, 0]$. Fig.5(b) plots σ_{xy} as a function of s for different values of maximum expansion order n. The discontinuity can be observed at $s/d = 1$.

To quantify the error introduced by the stress discontinuity, we define the following quantity as the maximum relative error of the stress jump at $s = d$,

$$\text{Discont} = \frac{||\sigma_{ij}(s = d^+) - \sigma_{ij}(s = d^-)||}{||\sigma_{ij}^{\text{WSL}}||} \tag{23}$$

The dependence of Discont on the maximum expansion order n is discussed in the next section.

3.3. Effect of maximum expansion order p

As indicated earlier, the present formulation of FMM is supposed to be applied to DD simulations, in which the derivatives of the Green's function are pre-computed up to order $n = p + 1$. It is important to know the necessary value for p to ensure that the relative error and discontinuities in the stress field are within a certain tolerance. The choice of how accurate the stress field needs to be in DD simulations is largely subjective. Given the approximations inherent in the DD model formulation, we assume an error of $\sim 5\%$ in stress calculations would usually be considered tolerable. In the following, we will determine the necessary value of p to achieve this level of accuracy.

Fig. 6(a) plots the relative error, RE, and discontinuity at cell boundary, Discont, as functions of p for the case of Mo at $L = 4d$. The values of RE and Discont in Mo are given

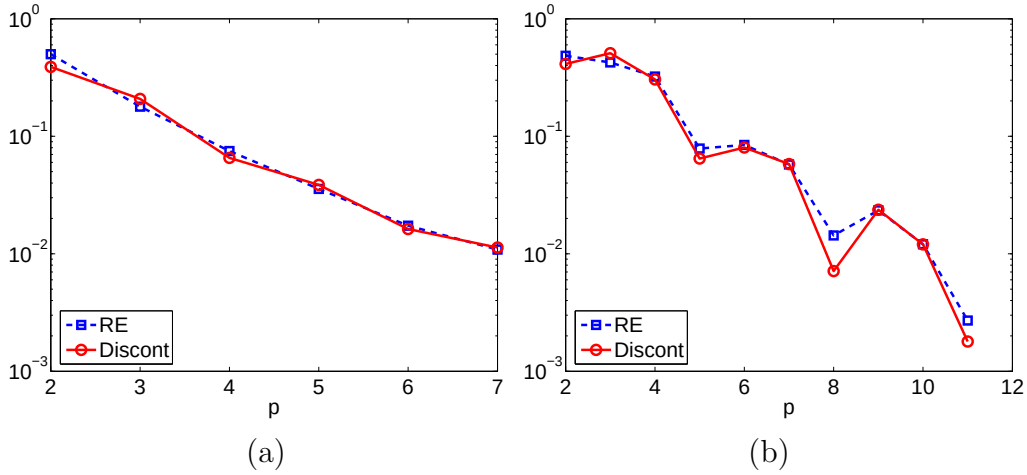

Figure 6. (a) The relative error, RE, and stress discontinuity at cell boundary, Discont, as functions of multipole expansion order p, for the case of Mo at $L = 4d$. (b) RE and Discont as functions of p for the case of Na at $L = 4d$.

below.

p	2	3	4	5	6	7
RE	50 %	18 %	7.5 %	3.6 %	1.7 %	1.1 %
Discont	39 %	21 %	6.6 %	3.9 %	1.6 %	1.1 %

It can be seen that $p \geq 5$ is sufficient to ensure that both RE and Discont are less than 5%, suggesting that the derivatives of the Green's function up to 7-th order need to be pre-computed for DD simulations in anisotropic Mo.

The maximum order of Green's function derivatives necessary to control the error within a specified tolerance depends on how anisotropic the crystal is. Fig. 6(b) plots RE and Discont as functions of p for the case of Na, which is highly anisotropic. The values are given below.

p	4	5	6	7	8	9	10	11
RE	32 %	7.9 %	8.4 %	5.8 %	1.4 %	2.3 %	1.2 %	0.3 %
Discont	30 %	6.5 %	8.0 %	5.8 %	0.7 %	2.3 %	1.2 %	0.2 %

It can be seen that $p \geq 8$ is sufficient to ensure that both RE and Discont are less than 5%, suggesting that the derivatives of the Green's function up to 10-th order need to be pre-computed for DD simulations in anisotropic Na.

4. Summary and discussion

We have developed a systematic procedure to derive the derivatives of the Green's function to arbitrary order in anisotropic elasticity. By pre-computing the high order derivatives of the Green's function, we performed multipole expansions of the dislocation stress field. The effect of the expansion orders on the relative error in the stress, as well as on the stress

discontinuity at cell boundaries, is investigated. For more anisotropic crystals, a higher expansion order is needed to reach the same level of accuracy.

The method described here is an important ingredient for the fast multipole method (FMM) in DD simulations with anisotropic elasticity. A full implementation of FMM requires a hierarchical cell structure and information passing between cells at different levels of the hierarchy. This has been implemented in the ParaDiS program within isotropic elasticity [4]. To extend this implementation to anisotropic elasticity, only the kernel connecting the multipole and the Taylor expansion coefficients needs to be changed to that described in this paper. While FMM enables $\mathcal{O}(N)$ scaling, the cell size needs to be chosen carefully according to the number of dislocation segments, as discussed in [4]. We note that for the FMM part of the dislocation force evaluation, the computational cost for anisotropic elasticity is similar to that for isotropic elasticity (within a factor of 10). This should be compared with the short range part of dislocation force evaluation, in which the computational cost for anisotropic elasticity is more than 200 times that for isotropic elasticity [9]. Therefore, it will be advantageous to shift more computations from the short range part to the FMM part (by reducing FMM cell size) in anisotropic elasticity DD simulations. This will reduce the gap in computational cost between DD simulations with isotropic and anisotropic elasticity.

Acknowledgments

We appreciate helpful discussions with Dr. Sylvie Aubry from Lawrence Livermore National Laboratory. JY and WC thank Prof. Eric Darve for valuable discussions on Section 2.3. We thank Mr. William P. Kuykendall for pointing out the pattern in the A_n^m coefficients in Appendix B. This work is made possible by the support from Lawrence Livermore National Laboratory and the Air Force Office of Scientific Research Grant No. FA9550-07-1-0464. SPF is supported by the European Communities under the contract of Association between EURATOM and CCFE. This work was carried out within the framework of the European Fusion Development Agreement. The views and opinions expressed herein do not necessarily reflect those of the European Commission. This work was also part-funded by the RCUK Energy Programme under grant EP/G003955.

Appendix A. Derivation of n-th order derivative of Green's function

For a maximum multipole expansion order p, the derivatives of the Green's function need to be pre-computed up to order $n = p + 1$. We evaluate the Green's function and its spatial derivatives based on the integral formalism [8, 15]. Unlike the matrix formalism, the integral formalism is numerically robust for elastic media with arbitrary symmetries (even including isotropic media) [8, 15]. The Green's function $G_{ij}(\boldsymbol{x} - \boldsymbol{x'})$ in an infinite elastic solid is the displacement in the i direction at a field point $\boldsymbol{x}$ due to a unit point force in the j direction

at $\boldsymbol{x'}$. It satisfies the equation

$$C_{ijkl}\frac{\partial^2}{\partial x_j \partial x_l}G_{km}(\boldsymbol{x}-\boldsymbol{x'}) + \delta_{im}\delta(\boldsymbol{x}-\boldsymbol{x'}) = 0. \tag{A.1}$$

Define the unit vector $\boldsymbol{T}$ in the direction of $(\boldsymbol{x}-\boldsymbol{x'})$ and consider a right-handed coordinate system $\boldsymbol{a}$-$\boldsymbol{b}$-$\boldsymbol{T}$, where $\boldsymbol{a}$ and $\boldsymbol{b}$ are also unit vectors (see Fig.A1). Introduce a unit vector $\boldsymbol{z}$, which makes an angle σ with $\boldsymbol{T}$, i.e.

$$\boldsymbol{z}\cdot\boldsymbol{T} = \cos\sigma \tag{A.2}$$

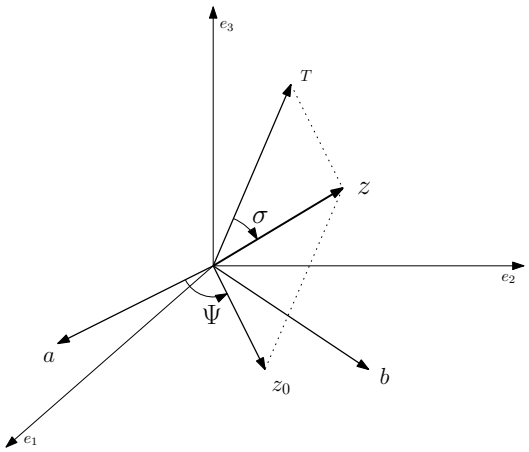

Figure A1. The unit vector $\boldsymbol{T}$ is along the direction of $(\boldsymbol{x}-\boldsymbol{x'})$. Unit vectors $\boldsymbol{a}$, $\boldsymbol{b}$ and $\boldsymbol{T}$ form a right-handed coordinate system. Unit vector $\boldsymbol{z}$ form an angle σ with $\boldsymbol{T}$. $\boldsymbol{z_0}$ is the projection of $\boldsymbol{z}$ on the $\boldsymbol{a}$-$\boldsymbol{b}$ plane and forms an angle Ψ with $\boldsymbol{a}$. If $\boldsymbol{z}$ lies on the $\boldsymbol{a}$-$\boldsymbol{b}$ plane, then $\sigma = \pi/2$.

For a given material with elastic stiffness tensor C_{ijkl}, the symmetric Christoffel stiffness matrix $M_{ir}(\boldsymbol{z})$ and its inverse $M^*_{ir}(\boldsymbol{z})$ are defined by

$$M_{ir}(\boldsymbol{z}) = C_{ijrs}z_j z_s \tag{A.3}$$

$$M^*_{ir}(\boldsymbol{z})M_{rm}(\boldsymbol{z}) = \delta_{im} \tag{A.4}$$

Equation (A.1) can be solved by Fourier transform [15], yielding

$$G_{ir}(\boldsymbol{x}-\boldsymbol{x'}) = \frac{1}{8\pi^3|\boldsymbol{x}-\boldsymbol{x'}|}\int_0^{2\pi}\mathrm{d}\Psi\int_0^{\pi}\mathrm{d}\sigma M^*_{ir}(\boldsymbol{z}(\Psi))\sin\sigma\int_0^{\infty}\mathrm{d}k\,\cos(k\cos\sigma), \tag{A.5}$$

where Ψ is a polar angle in the plane $\boldsymbol{z}\cdot\boldsymbol{T}=0$. The Green's function can be further simplified to

$$G_{ir}(\boldsymbol{x}-\boldsymbol{x'}) = \frac{1}{8\pi^2|\boldsymbol{x}-\boldsymbol{x'}|}\int_0^{2\pi}M^*_{ir}(\boldsymbol{z}(\Psi))\,\mathrm{d}\Psi, \tag{A.6}$$

where the integral must be evaluated in the plane $\boldsymbol{z}\cdot\boldsymbol{T}=0$, i.e. $\sigma=\pi/2$. For arbitrary orthonormal vectors $\boldsymbol{a}$ and $\boldsymbol{b}$ in the plane $\boldsymbol{z}\cdot\boldsymbol{T}=0$, the vector $\boldsymbol{z}$ can be given by

$$\boldsymbol{z} = \boldsymbol{a}\cos\Psi + \boldsymbol{b}\sin\Psi \tag{A.7}$$

Expressions for the first and second derivatives of the Green's function were derived by Barnett [15]. Willis [16] demonstrated a way to derive the n-th order derivative of the Green's function. However, his expressions are difficult to use in a numerical implementation. Here we provide an alternative derivation which is more suitable for numerical calculations. Using the methods in [15], the n-th derivative of the Green's function can be shown to have the form

$$\frac{\partial^{(n)} G_{ir}(\boldsymbol{x}-\boldsymbol{x'})}{\partial x_s \partial x_m \dots \partial x_p} = \frac{1}{8\pi^3 |\boldsymbol{x}-\boldsymbol{x'}|^{n+1}} \int_0^{2\pi} \mathrm{d}\Psi \int_0^{\pi} \mathrm{d}\sigma \sin\sigma \, [M^*_{ir}(\boldsymbol{z})\, z_s z_m \dots z_p] \cdot \frac{\mathrm{d}^n}{\mathrm{d}\,(\cos\sigma)^n} \int_0^{\infty} \mathrm{d}k \, \cos(k\cos\sigma) \tag{A.8}$$

Since

$$\int_0^{\infty} dk \cos(k\cos\sigma) = \pi\delta(\cos\sigma) \tag{A.9}$$

we have

$$\frac{\partial^{(n)} G_{ir}(\boldsymbol{x}-\boldsymbol{x'})}{\partial x_s \partial x_m \dots \partial x_p} = \frac{1}{8\pi^2 |\boldsymbol{x}-\boldsymbol{x'}|^{n+1}} \int_0^{2\pi} \mathrm{d}\Psi \cdot \cdot \int_0^{\pi} \mathrm{d}\sigma \sin\sigma \, [M^*_{ir}(\boldsymbol{z})\, z_s z_m \dots z_p] \, \frac{\mathrm{d}^n}{\mathrm{d}\,(\cos\sigma)^n} \delta(\cos\sigma) \tag{A.10}$$

Define $u \equiv \cos\sigma$, then $\mathrm{d}u = -\sin\sigma\,\mathrm{d}\sigma$. Denote $F_n(u) = M^*_{ir}(\boldsymbol{z})\, z_s z_m \dots z_p$, the inner integral over the polar angle σ becomes (see Lighthill [17])

$$\int_{-1}^{1} \mathrm{d}u \, F_n(u) \frac{\mathrm{d}^n \delta(u)}{\mathrm{d}\,u^n} = (-1)^n \left. \frac{\partial^n F_n(u)}{\partial\, u^n} \right|_{u=0} \tag{A.11}$$

Therefore,

$$\frac{\partial^{(n)} G_{ir}(\boldsymbol{x}-\boldsymbol{x'})}{\partial x_s \partial x_m \dots \partial x_p} = \frac{(-1)^n}{8\pi^2 |\boldsymbol{x}-\boldsymbol{x'}|^{n+1}} \int_0^{2\pi} \mathrm{d}\Psi \left\{ \frac{\partial^n}{\partial\, u^n} [M^*_{ir}(\boldsymbol{z})\, z_s z_m \dots z_p] \right\}_{u=0} \tag{A.12}$$

One can show that the integrand is a periodic function of Ψ with period π. Hence,

$$\begin{aligned} \frac{\partial^{(n)} G_{ir}(\boldsymbol{x}-\boldsymbol{x'})}{\partial x_s \partial x_m \dots \partial x_p} &= \frac{(-1)^n}{4\pi^2 |\boldsymbol{x}-\boldsymbol{x'}|^{n+1}} \int_0^{\pi} \mathrm{d}\Psi \left\{ \frac{\partial^n}{\partial\, u^n} [M^*_{ir}(\boldsymbol{z})\, z_s z_m \dots z_p] \right\}_{u=0} \\ &= \frac{1}{4\pi^2 |\boldsymbol{x}-\boldsymbol{x'}|^{n+1}} \int_0^{\pi} \mathrm{d}\Psi \left\{ \left(\frac{1}{\sin\sigma} \frac{\partial}{\partial\,\sigma} \right)^n [M^*_{ir}(\boldsymbol{z}) z_s z_m \dots z_p] \right\}_{\sigma=\pi/2} \end{aligned} \tag{A.13}$$

When $n = 0$, 1, 2, the results above are identical to those given by Barnett [15]. Here we give the explicit expression for the third derivative of Green's function:

$$\begin{aligned} \frac{\partial^3 G_{ir}(\boldsymbol{x}-\boldsymbol{x'})}{\partial x_s \partial x_m \partial x_p} &= \frac{1}{4\pi^2 |\boldsymbol{x}-\boldsymbol{x'}|^4} \int_0^{\pi} \mathrm{d}\Psi \left[\left(\frac{1}{\sin\sigma} \frac{\partial}{\partial\,\sigma} \right)^3 (M^*_{ir}(\boldsymbol{z}) z_s z_m z_p) \right]_{\sigma=\pi/2} \\ &= \frac{1}{4\pi^2 |\boldsymbol{x}-\boldsymbol{x'}|^4} \int_0^{\pi} \mathrm{d}\Psi \left[\frac{\partial}{\partial\,\sigma} F_3(\sigma) + \frac{\partial^3}{\partial\,\sigma^3} F_3(\sigma) \right]_{\sigma=\pi/2} \end{aligned} \tag{A.14}$$

where $F_3(\sigma) = M^*_{ir}(\boldsymbol{z})\, z_s z_m z_p$. To calculate the third order derivative of the Green's function, we need to compute $\partial F_3(\sigma)/\partial\sigma$ and $\partial^3 F_3(\sigma)/\partial\sigma^3$, as described in Appendix B.

Because spatial derivatives are independent of the order in which they are taken, a more compact way to represent (and store) high order derivatives of the Green's function is the following.

$$\left(\frac{\partial}{\partial x_1}\right)^a \left(\frac{\partial}{\partial x_2}\right)^b \left(\frac{\partial}{\partial x_3}\right)^c G_{ir}(\boldsymbol{x}-\boldsymbol{x'})$$

$$= \frac{(-1)^{a+b+c}}{4\pi^2|\boldsymbol{x}-\boldsymbol{x'}|^{a+b+c+1}} \int_0^\pi \mathrm{d}\Psi \left\{ \left(\frac{\partial}{\partial\, u}\right)^{a+b+c} \left[M^*_{ir}(\boldsymbol{z})\cdot(z_1)^a(z_2)^b(z_3)^c\right] \right\}_{u=0} \tag{A.15}$$

$$= \frac{1}{4\pi^2|\boldsymbol{x}-\boldsymbol{x'}|^{a+b+c+1}} \int_0^\pi \mathrm{d}\Psi \left\{ \left(\frac{1}{\sin\sigma}\frac{\partial}{\partial\,\sigma}\right)^{a+b+c} \left[M^*_{ir}(\boldsymbol{z})\cdot(z_1)^a(z_2)^b(z_3)^c\right] \right\}_{\sigma=\pi/2} \tag{A.16}$$

More explicit expressions of the Green's function derivatives can be obtained by following either equation (A.15) or equation (A.16). In Appendix B, we use equation (A.16), following the approach of Barnett [15]. However, this approach requires the expression of $(\frac{1}{\sin\sigma}\frac{\partial}{\partial\sigma})^n$ in terms of $(\frac{\partial}{\partial\sigma})^m$, $m = 1, \cdots, n$. In Appendix C, we use equation (A.15), which bypasses this complication. We have implemented both methods described in Appendix B and Appendix C and they give identical numerical results.

Appendix B. Numerical algorithm based on $(\partial/\partial\sigma)^m$

From Appendix A, the calculation of the n-th order derivative of the Green's function amounts to the calculations of the m-th order derivatives of $F_n(\sigma)$, with $m = 0, 1, \cdots, n$. Below is a procedure to compute the m-th order ($m \le n$) derivative of $F_n(\sigma) \equiv M^*_{ir}(\boldsymbol{z}) z_s z_m \ldots z_p$, and subsequently the n-th derivative of the Green's function. Recall that we only need to evaluate these derivatives at $\sigma = \pi/2$. However, the substitution of $\sigma = \pi/2$ can only be made after taking the derivatives.

(I) Compute m-th order derivatives of $M_{ir}(\boldsymbol{z})$ for $m = 0, 1, \cdots, n$.

For example, starting from equation (A.3), we obtain

$$\frac{\partial M_{ir}}{\partial\,\sigma} = C_{iprw}\left(z_p\frac{\partial z_w}{\partial\sigma} + z_w\frac{\partial z_p}{\partial\sigma}\right) \tag{B.1}$$

$$\frac{\partial^2 M_{ir}}{\partial\,\sigma^2} = C_{iprw}\left(2\frac{\partial z_p}{\partial\sigma}\frac{\partial z_w}{\partial\sigma} + z_w\frac{\partial^2 z_p}{\partial\sigma^2} + z_p\frac{\partial^2 z_w}{\partial\sigma^2}\right) \tag{B.2}$$

$$\frac{\partial^3 M_{ir}}{\partial\,\sigma^3} = C_{iprw}\left(z_p\frac{\partial^3 z_w}{\partial\sigma^3} + 3\frac{\partial z_p}{\partial\sigma}\frac{\partial^2 z_w}{\partial\sigma^2} + 3\frac{\partial^2 z_p}{\partial\sigma^2}\frac{\partial z_w}{\partial\sigma} + \frac{\partial^3 z_p}{\partial\sigma^3}z_w\right) \tag{B.3}$$

Equations (B.1-B.3) take forms similar to the binomial expansion with binomial coefficient

C_n^k, and indeed can be generalized to arbitrary order, *i.e.*,

$$\frac{\partial^m M_{ir}}{\partial\,\sigma^m} = C_{iprw} \sum_{k=0}^{m} C_m^k \,\frac{\partial^k z_p}{\partial \sigma^k}\,\frac{\partial^{m-k} z_w}{\partial \sigma^{m-k}} \tag{B.4}$$

$$C_m^k \quad \equiv \frac{m!}{k!(m-k)!} \tag{B.5}$$

From Fig. A1, the derivatives of $\boldsymbol{z}$ with respect to σ to arbitrary order can be obtained from the following relations at $\sigma = \pi/2$.

$$\left\{\frac{\partial z_s}{\partial \sigma}\right\}_{\sigma=\pi/2} = -T_s, \quad \left\{\frac{\partial^2 z_s}{\partial \sigma^2}\right\}_{\sigma=\pi/2} = -z_s,$$
$$\left\{\frac{\partial^3 z_s}{\partial \sigma^3}\right\}_{\sigma=\pi/2} = T_s, \quad \left\{\frac{\partial^4 z_s}{\partial \sigma^4}\right\}_{\sigma=\pi/2} = z_s. \tag{B.6}$$

Equations (B.4-B.6) are sufficient to provide explicit expressions for the derivatives of $M_{ir}(\boldsymbol{z})$ to arbitrary order. For example,

$$\frac{\partial M_{ir}}{\partial\,\sigma} = C_{iprw}(-z_p T_w - z_w T_p) \tag{B.7}$$

$$\frac{\partial^2 M_{ir}}{\partial\,\sigma^2} = C_{iprw}(2T_p T_w - 2z_p z_w) \tag{B.8}$$

$$\frac{\partial^3 M_{ir}}{\partial\,\sigma^3} = C_{iprw}(4z_p T_w + 4T_p z_w) \tag{B.9}$$

(II) Compute m-th order derivatives of $M^*_{ir}(\boldsymbol{z})$ for $m = 0, 1, \cdots, n$.

Indices are suppressed for clarity. Noting that $MM^* = I$, we have, for $m > 0$,

$$\begin{aligned} 0 &= \frac{\partial^m}{\partial\,\sigma^m}\,(MM^*) \\ &= \frac{\partial^m M}{\partial\,\sigma^m} + C_m^1 \frac{\partial^{m-1} M}{\partial\,\sigma^{m-1}}\frac{\partial M^*}{\partial\,\sigma} + \cdots + C_m^{m-1}\frac{\partial M}{\partial\,\sigma}\frac{\partial^{m-1} M^*}{\partial \sigma^{m-1}} + \frac{\partial^m M^*}{\partial \sigma^m} \end{aligned} \tag{B.10}$$

Therefore,

$$\frac{\partial^m M^*}{\partial \sigma^m} = -\sum_{k=0}^{m-1} C_m^k \,\frac{\partial^{m-k} M}{\partial\,\sigma^{m-k}}\,\frac{\partial^k M^*}{\partial\,\sigma^k} \tag{B.11}$$

This allows the m-th order derivative of M^* to be computed from lower order derivatives.

(III) Compute m-th order derivatives of $(z_1)^a(z_2)^b(z_3)^c$ for $m = 1, \cdots, n$.

This can also be computed recursively from a binomial expansion. Obviously, the derivative is zero if $a = b = c = 0$. Without loss of generality, let us assume $c > 0$. Then,

$$\frac{\partial^m}{\partial\,\sigma^m}\left[(z_1)^a(z_2)^b(z_3)^c\right] = \sum_{k=0}^{m} C_m^k \left\{\frac{\partial^{m-k}}{\partial\,\sigma^{m-k}}\left[(z_1)^a(z_2)^b(z_3)^{c-1}\right]\right\}\frac{\partial^k z_3}{\partial\,\sigma^k}, \tag{B.12}$$

This means that the derivatives of $(z_1)^a(z_2)^b(z_3)^c$ can be constructed from the derivatives of $(z_1)^{a'}(z_2)^{b'}(z_3)^{c'}$, where $a'+b'+c' = a+b+c-1$.

(IV) Compute m-th order derivatives of $F_n(\sigma)$ for $m = 1, \cdots, n$.

Recall that

$$F_n(\sigma) = \left[M^*_{ir}(\boldsymbol{z})\,(z_1)^a(z_2)^b(z_3)^c\right] \tag{B.13}$$

where $a+b+c = n$. Obviously, F_n depends on the specific values of a, b, c, but for brevity this dependence is not written out explicitly. Again, the derivatives of F_n can be expressed from the results obtained from previous steps using the binomial expansion.

$$\frac{\partial^m}{\partial\,\sigma^m}F_n(\sigma) = \sum_{k=0}^{m} C_m^k \left[\frac{\partial^{m-k}}{\partial\,\sigma^{m-k}}M^*_{ir}(\boldsymbol{z})\right] \frac{\partial^k}{\partial\,\sigma^k}\left[(z_1)^a(z_2)^b(z_3)^c\right] \tag{B.14}$$

(V) Compute $(\frac{1}{\sin\sigma}\frac{\partial}{\partial\sigma})^n F_n(\sigma)$ from $(\frac{\partial}{\partial\sigma})^m F_n(\sigma)$ for $m = 1, \cdots, n$.

This step is necessary because the integrand in equation (A.16) contains $(\frac{1}{\sin\sigma}\frac{\partial}{\partial\sigma})^n$ instead of $(\frac{\partial}{\partial\sigma})^n$. This would not be necessary if we followed equation (A.15), as described in Appendix C.

In general, we have the following relationship at $\sigma = \pi/2$,

$$\left(\frac{1}{\sin\sigma}\frac{\mathrm{d}}{\mathrm{d}\sigma}\right)^n F_n(\sigma) = \sum_{m=1}^{n} A_n^m \cdot \frac{\partial^m}{\partial\,\sigma^m}F_n(\sigma) \tag{B.15}$$

The coefficients A_n^m can be computed efficiently using a symbolic manipulator with the following procedure. Consider an arbitrary function $f(\sigma)$, which is Taylor-expanded around $\sigma = \pi/2$. Define $\beta = \pi/2 - \sigma$.

$$f(\sigma) = a_0 + a_1\,\beta + \frac{a_2}{2!}\,\beta^2 + \frac{a_3}{3!}\,\beta^3 + \cdots \tag{B.16}$$

where $a_n = (-\frac{\partial}{\partial\sigma})^n f(\sigma)|_{\sigma=\pi/2}$. Since $u = \cos\sigma$, we have $\sigma = \arccos(u)$ and f can also be written as a function of u, which can be Taylor expanded around $u = 0$.

$$f(u) = b_0 + b_1\,u + \frac{b_2}{2!}\,u^2 + \frac{b_3}{3!}\,u^3 + \cdots \tag{B.17}$$

where $b_n = (\frac{\partial}{\partial u})^n f(u)|_{u=0}$. We can also Taylor expand $\beta = \pi/2 - \arccos(u)$ around $u = 0$, which gives

$$\beta = u + \frac{1}{6}\,u^3 + \frac{3}{40}\,u^5 + \frac{5}{112}\,u^7 + \frac{35}{1152}\,u^9 + \frac{63}{2816}\,u^{11} + \mathcal{O}(u^{13}) \tag{B.18}$$

Substituting equation (B.18) into equation (B.16) and comparing the result with equation (B.17), we obtain

$$\begin{aligned} b_1 &= a_1 \\ b_2 &= a_2 \\ b_3 &= a_1 + a_3 \end{aligned}$$

$$
\begin{aligned}
b_4 &= 4\,a_2 + a_4 \\
b_5 &= 9\,a_1 + 10\,a_3 + a_5 \\
&\cdots
\end{aligned}
$$

The coefficients linking b_n and a_m are A_n^m. The values of A_n^m for n from 1 to 12 are listed below. It takes about one minute to compute all these coefficients using Matlab.

n	$m=1$	2	3	4	5	6	7	8	9	10	11	12
1	1											
2	0	1										
3	1	0	1									
4	0	4	0	1								
5	9	0	10	0	1							
6	0	64	0	20	0	1						
7	225	0	259	0	35	0	1					
8	0	2304	0	784	0	56	0	1				
9	11025	0	12916	0	1974	0	84	0	1			
10	0	147456	0	52480	0	4368	0	120	0	1		
11	893025	0	1057221	0	172810	0	8778	0	165	0	1	
12	0	14745600	0	5395456	0	489280	0	16368	0	220	0	1

For example, the $n=3$ entry in the above table gives

$$\left(\frac{1}{\sin\sigma}\frac{\mathrm{d}}{\mathrm{d}\sigma}\right)^3 F_3(\sigma) = \frac{\partial^3}{\partial\,\sigma^3}F_3(\sigma) + \frac{\partial}{\partial\,\sigma}F_3(\sigma) \tag{B.19}$$

which is consistent with equation (A.14).

We note (without proof) that the coefficients A_n^m obey interesting patterns. For example, $A_n^n = 1$ and $A_n^m = 0$ if $m+n$ is odd.

$$
\begin{aligned}
A_n^1 &= (1)^2, \quad (1\times 3)^2, \quad (1\times 3\times 5)^2, \cdots, \qquad \text{for } n = 3,5,7,\cdots \\
A_n^2 &= (2)^2, \quad (2\times 4)^2, \quad (2\times 4\times 6)^2, \cdots, \qquad \text{for } n = 4,6,8,\cdots \\
A_{m+2}^m &= A_{m+1}^{m-1} + \frac{m(m+1)}{2}, \quad \text{starting with} \quad A_3^1 = 1
\end{aligned}
\tag{B.20}
$$

Steps (I)-(V) above compute the integrand in the expression for the arbitrary derivatives of the Green's function, equation (A.16). The integral itself is performed numerically using a uniform grid [9]. Let N_{int} be the number of integration points. The grid points are,

$$\Psi_i = \frac{i}{N_{\text{int}}}\cdot\pi\,, \quad i = 0,1,\cdots,N_{\text{int}}-1 \tag{B.21}$$

Because of the periodic nature of the integrand, a rectangular rule is used for numerical quadrature.

The time it takes Matlab to evaluate all components of Green's function derivatives up to order n for a given vector $\boldsymbol{x}-\boldsymbol{x}' = [1\,0\,0]$ and $N_{\text{int}} = 21$ is given below. The time to evaluate the coefficients A_n^m is not included here.

n	1 to 4	5	6	7	8	9	10	11	12
time (seconds)	< 1	2	3	6	11	18	29	46	72

Appendix C. Numerical algorithm based on $(\partial/\partial u)^m$

The algorithm based on equation (A.15) is very similar to that described in Appendix B, with $\partial/\partial\sigma$ replaced by $\partial/\partial u$. There are only two key differences. First, the expressions for $\partial^m z_s/\partial u^m$ are different from $\partial^m z_s/\partial\sigma^m$. Second, Step (V) is no longer necessary. For clarity, in the following, we list the four steps for computing Green's function derivatives based on equation (A.15).

(I) Compute m-th order derivatives of $M_{ir}(\boldsymbol{z})$ for $m = 0, 1, \cdots, n$.

$$\frac{\partial^m M_{ir}}{\partial\, u^m} = C_{iprw} \sum_{k=0}^{n} C_m^k \frac{\partial^k z_p}{\partial u^k} \frac{\partial^{m-k} z_w}{\partial u^{m-k}} \tag{C.1}$$

To develop the expressions for $\partial^m z_s/\partial u^m$, we need to consider the general case where $\boldsymbol{z}$ no longer lies in the plane $\boldsymbol{z}\cdot\boldsymbol{T} = 0$. In this case,

$$\begin{aligned} \boldsymbol{z} &= (\boldsymbol{a}\cos\Psi + \boldsymbol{b}\sin\Psi)\cdot\sin\sigma + \boldsymbol{T}\cdot\cos\sigma \\ &= (\boldsymbol{a}\cos\Psi + \boldsymbol{b}\sin\Psi)\cdot\sqrt{1-u^2} + \boldsymbol{T}\cdot u \end{aligned} \tag{C.2}$$

Therefore

$$\left\{\frac{\partial z_s}{\partial\, u}\right\}_{u=0} = z_s \left.\frac{\mathrm{d}\sqrt{1-u^2}}{\mathrm{d}\, u}\right|_{u=0} + T_s = T_s \tag{C.3}$$

$$\left\{\frac{\partial^2 z_s}{\partial\, u^2}\right\}_{u=0} = z_s \left.\frac{\mathrm{d}^2\sqrt{1-u^2}}{\mathrm{d}\, u^2}\right|_{u=0} = -z_s \tag{C.4}$$

Define

$$B_m \equiv \left.\frac{\mathrm{d}^m\sqrt{1-u^2}}{\mathrm{d}\, u^m}\right|_{u=0} \tag{C.5}$$

we have

$$\left\{\frac{\partial^m z_s}{\partial\, u^m}\right\}_{u=0} = z_s\, B_m + T_s\, \delta_{m,1} \tag{C.6}$$

Coefficients B_m can be evaluated by a symbolic manipulator (*e.g.* Matlab), which gives

m	1	2	3	4	5	6	7	8	9	10	11	12
B_m	0	-1	0	-3	0	-45	0	-1575	0	-99925	0	-9823275

The B_m are easier to evaluate than the A_n^m coefficients needed in Appendix B.

(II) Compute m-th order derivatives of $M^*_{ir}(\boldsymbol{z})$ for $m = 0, 1, \cdots, n$.

$$\frac{\partial^m M^*}{\partial u^m} = -\sum_{k=0}^{m-1} C_m^k \frac{\partial^{m-k} M}{\partial u^{m-k}} \frac{\partial^k M^*}{\partial u^k} \tag{C.7}$$

(III) Compute m-th order derivatives of $(z_1)^a(z_2)^b(z_3)^c$ for $m = 1, \cdots, n$.

$$\frac{\partial^m}{\partial u^m}\left[(z_1)^a(z_2)^b(z_3)^c\right] = \sum_{k=0}^{m} C_m^k \left\{\frac{\partial^{m-k}}{\partial u^{m-k}}\left[(z_1)^a(z_2)^b(z_3)^{c-1}\right]\right\} \frac{\partial^k z_3}{\partial u^k}, \tag{C.8}$$

assuming $c > 0$.

(IV) Compute m-th order derivatives of $F_n(u)$ for $m = 1, \cdots, n$.

$$\frac{\partial^m}{\partial u^m} F_n(u) = \sum_{k=0}^{m} C_m^k \left[\frac{\partial^{m-k}}{\partial u^{m-k}} M_{ir}^*(\boldsymbol{z})\right] \frac{\partial^k}{\partial u^k}\left[(z_1)^a(z_2)^b(z_3)^c\right] \tag{C.9}$$

Steps (I)-(IV) above compute the integrand in the expression for the arbitrary derivatives of the Green's function, equation (A.15). The integral itself is performed numerically on a uniform grid in the same way as in Appendix B. The computational time for the method described in this Appendix is essentially the same as that for the method described in Appendix B.

References

[1] L. Greengard, V. Rokhlin, *A fast algorithm for particle simulations*, Journal of Computational Physics, **73**, 325-348 (1987)

[2] R. LeSar, J.M. Rickman, *Multipole expansion of dislocation interactions: Application to discrete dislocations*, Physical Review B, **65**, 144110 (2002)

[3] Z. Wang, N. Ghoniem, R. LeSar, *Multipole representation of the elastic field of dislocation ensembles*, Physical Review B, **69**, 174102 (2004)

[4] A. Arsenlis, W. Cai, M. Tang, M. Rhee, T. Oppelstrup, G. Hommes, T. G. Pierce, V. V. Bulatov, *Enabling strain hardening simulations with dislocation dynamics*, Modelling Simul. Mater. Sci. Eng. **15**, 553 (2007)

[5] Greengard L., Rockhlin V, *A new version of the Fast Multipole Method for the Laplace equation in three dimensions*, Acta Numer. **6**, 229-69 (1997)

[6] D. Zhao, J. Huang, Y. Xiang, *A new version fast multipole method for evaluating the stress field of dislocation ensembles*,Modelling Simul. Mater. Sci. Eng. **18**, 45006 (2010)

[7] S. P. Fitzgerald, *FrankRead sources and the yield of anisotropic cubic crystals*, Philos. Mag. Lett. **90**, 209 (2010)

[8] D. J. Bacon, D. M. Barnett and R. O. Scattergood, *Anisotropic continuum theory of lattice defects*, Prog. Mater. Sci. **23** 51262 (1979)

[9] J. Yin, D. M. Barnett and W. Cai, *Efficient computation of forces on dislocation segments in anisotropic elasticity*, Modelling Simul. Mater. Sci. Eng. **18**, 45013 (2010)

[10] J. Lothe, Dislocations in Anisotropic Media, in Elastic Strain Fields and Dislocation Mobility, V. L. Indenbom and J. Lothe, ed., in the series of Modern Problems in Condensed Matter Physics, v. 31, (North-Holland, Amsterdam, 1992)

[11] L. Pang, *A New O(N) Method for Modeling and Simulating the Behavior of a Large Number of Dislocations in Anisotropic Linear Elastic Media*, PhD thesis, Stanford University (2001)

[12] J. P. Hirth and J. Lothe, *Theory of Dislocations*, 2nd ed. (Wiley, New York, 1982) (p.101)

[13] C. R. Weinberger, W. Cai and D. M. Barnett, *Elasticity of Microscopic Structures*, Lecture Notes for ME340B, `http://micro.stanford.edu/~caiwei/me340b` (p.98)

[14] The Matlab programs implementing the algorithms in this paper can be downloaded at `http://micro.stanford.edu/~caiwei/Forum`

[15] D. M. Barnett, *The Precise Evaluation of Derivatives of the Anisotropic Elastic Green's Functions*, phys. stat. sol. (b) **49**, 741 (1972)

[16] J. R. Willis, *The Interaction of Gas Bubbles in an Anisotropic Elastic solid*, J. Mech. Phys. Solids, **23**, 129-138 (1975)

[17] M. J. Lighthill, *An Introduction to Fourier Analysis and Generalised Functions*, (Cambridge University Press, 1958) p. 19, eqn. (17)